RSC Advances

Quercetin delivery to porcine cornea and sclera by solid lipid nanoparticles and nanoemulsion

Journal:	*RSC Advances*
Manuscript ID	RA-ART-08-2015-017423.R1
Article Type:	Paper
Date Submitted by the Author:	24-Oct-2015
Complete List of Authors:	Liu, Chi-Hsien; Chang Gung Univ, IBBE Huang, Yun-Chun; Chang Gung Univ, IBBE Jhang, Jhe Wei; CGU Liu, Yu-Hong; CGU Wu, Wei-chi; Chang Gung Univ,
Subject area & keyword:	Nanomedicine < Nanoscience

Quercetin delivery to porcine cornea and sclera by solid lipid nanoparticles and nanoemulsion

Chi-Hsien Liu[*1,2,3], Yun-Chun Huang[1], Jhe-Wei Jhang[1], Yu-Hing Liu[1], Wei-Chi Wu[4,5]

[1] Graduate Institute of Biochemical and Biomedical Engineering, Chang Gung University, 259, Wen-Hwa first Road, Kwei-Shan, Tao-Yuan 333, Taiwan

[2] Center for Biomedical Engineering, Chang Gung University, 259, Wen-Hwa first Road, Kwei-Shan, Tao-Yuan 333, Taiwan

[2] Research Center for Industry of Human Ecology, Chang Gung University of Science and Technology, Taoyuan, Taiwan

[4] College of Medicine, Chang Gung University, Taoyuan, Taiwan

[5] Department of Ophthalmology, Chang Gung Memorial Hospital, Taoyuan, Taiwan

Quercetin is a flavonoid having a strong antioxidant capacity. Recent studies indicate that quercetin can protect eye cells from oxidative damage. Lipid nanocarriers can protect the lipophilic drugs, achieving greater physical and chemical stability and controlling the release. Two potential nanocarriers including nanoemulsions (NE) and solid lipid nanoparticles (SLNs) are chosen as vehicles for quercetin encapsulation. Biocompatible surfactants Tween and Span were combined to develop oil in water interfaces to stabilize the quercetin. The size distribution of lipid nanocarriers was around 150~345 nm by using Dynamic Light Scattering or Transmission Electron Microscopy. The ocular quercetin delivery was confirmed by using confocal microscopy and *ex vivo* porcine eyes. The quercetin loaded solid lipid nanoparticles had the highest flux of 158 μg cm^{-2} on cornea after 24 hours. In addition, SLNs had the lowest cytotoxicity for cornea and retinal ganglion cells, and the value of half maximal inhibitory concentration were 268.85 and 211.3 μg ml^{-1}, respectively. Quercetin loaded SLNs could efficiently protect cornea and retinal ganglion cells from H_2O_2-induced oxidative damages. Taken together, our results help to shed light on the complex interplay between the quercetin, the carrier composition, the ocular tissues and the antioxidant activities.

Keyword: quercetin, lipid nanocarriers, antioxidant, ocular delivery

1. Introduction

The topical application of eye drops on the eye activates lacrimation and tear turnover which cause dilution and drainage of the drug[1]. Additionally, conjunctival blood capillaries and lymphatics can cause significant drug loss into the systemic circulation. The anatomical barriers including tear film and cornea also attribute

to the low drug bioavailability in the intraocular tissues[2]. Therefore, a new delivery system that can enhance the efficacy of ocular delivery is needed for the patients. Lipid based nanocarriers composed by biodegradable ingredients which can act as carriers of different hydrophobic drugs at the nano-scale. Advantages of the lipid-based nanocarriers for the topical ocular delivery can be summarized as follows[3]. Lipid-based nanocarriers might be act as a bio-mimic tear film since the lipid prevents the evaporation of the aqueous layer and lubricates the eyeball. Lipid components in the lipid-based nanocarriers can interact with the lipid layer of the tear film, enabling the carriers to adhere in the conjunctival sac as a drug depot for a long time. The surfactant, another ingredient, functions as a drug penetration enhancer to increase drug delivery. By virtues of their nanoscale and high surface/volume ratio, nanocarriers overcome the physiological barriers and enhance the bioavailability [4]. For example, solid lipid nanoparticles (SLNs) can accommodate lipophilic drugs in the core of the lipid matrix and can be easily produced on a large scale without using the organic solvents [5, 6]. The residence time of tobramycin in SLNs is longer than the eye drop control when applied in rabbit eyes[7]. Other reports have also shown the extended residence on the ocular surface by using drug-loaded lipid nanocarriers [8]. The above cited work provides a base line for the lipid nanoparticles and revel that SLNs will be useful to elevate the therapeutic efficacy of drugs in ocular diseases.

Since the oxidative stress is a major factor in ocular inflammatory diseases, antioxidants or reactive oxygen scavengers are potent in the therapeutic application[9]. Quercetin has been intensively studied because it's sound anti-inflammation, anticancer and antioxidant properties[10, 11]. Quercetin might be useful to reduce the oxidative stress involved in the formation of senile cataract which is the most common age-related eye complication [12]. The damage of retinal epithelia related to age-related macular degeneration (ADME) can be protected by quercetin. This protection mechanisms are involved in the inhibition of pro-inflammatory factor (IL-6) synthesis by inducing the expression of ROS-catalyzing proteins[13]. Additionally, the murine uveitis models indicate the anti-inflammatory potentials of quercetin in suppression of intraocular inflammation induced by retinal S antigen[14]. However, the instability of quercetin result in poor bioavailability, poor permeability and extensive first pass metabolism by using the oral administration [10]. Quercetin has been encapsulated in different nanocarriers using various techniques such as, microemulsions are designed as quercetin vehicles for transdermal[15] and pulmonary delivery [16]. In order to increase the intestinal absorption of quercetin, the vehicles such as SLNs [17] and microemulsion [18] have been found to be potential carriers for the oral delivery. Additionally, SLNs improve quercetin permeation across the blood-brain barrier by the intravenous administration and enhance the therapeutic efficacy of this drug in Alzheimer's disease[19].

Researchers have demonstrated the lipid nanocarriers are potent vehicles for quercetin delivery. However, rare studies have evaluated the effect of lipid-based nanocarriers on ocular quercetin delivery to the best of our knowledge. Ocular drug delivery is one of the most challenging fields because of the critical restrict and specific environment of the eyes[20]. Since partition data for quercetin loaded nanoparticles in the ocular (scleral or corneal) tissues are limited and the influences of quercetin to ocular accumulation on the transport behavior of quercetin have not been systematically studied. Therefore, keeping in this view an attempt has been made to characterize the nano-scaled lipid vehicles including the microstructure, encapsulation, size distribution and zeta potential and also to determine the partition coefficients and quercetin accumulation in the porcine sclera and cornea. Additionally, the antioxidant activities of quercetin loaded nanoparticles and biocompatibility in two ocular cell lines were carried out. The results in present study could be applied to understand the roles of the lipid composition on the accumulation of quercetin in the ocular tissues.

2. Materials and Methods

2.1. Materials

Quercetin was provided by Wako Co (Japan). Fresh porcine eyes were donated by Ya-Shin Pork Industry and Tong-Ying Co. (Taoyuan, Taiwan). Compritol 888, a glyceryl palmitostearate, was donated by Gattefossé Co. (N.J., USA). Estasan (a caprylic- and capric-triglyceride) was provided by Uniqema (Brombough, UK). Tween 40 was purchased from IL-Shin Surfactant Co. (Seoul, Korea). Sephadex G-50 was provided by GE Healthcare (England). Ethanol, methanol, tetrahydrofuran, acetic acid, Span 40 and other chemicals were purchased from Sigma-Aldrich, unless otherwise stated. All reagents were used as received, without further purification.

2.2. Preparation and characterization of quercetin-laden lipid vehicles

Lipid vehicles were prepared using the previous method [21]. In brief, aqueous and oil phases were separately prepared. Lipid, quercetin, and surfactants were melted at 75℃ to prevent the crystallization of lipids. Water was heated at 75℃ and added to the melted oil phase. The mixture was then dispersed with an ultrasonic probe (XL2000, Misonic, NY, USA) for 7 min. Finally, the nanocarriers were used for further test after cooling down at room temperature for 12 hours. Compritol in SLNs and Estasan in NE were fixed at the concentration of 2.0 %. The composition of lipid vehicles was shown in Table 1. Brookfield viscometer (DV II+, Brookfield, Stoughton, MA, USA) was employed for viscosity determination of the lipid nanocarriers. Surface tension measurements were carried out at room temperature using Contact Angle Analyzer (SEO Phonex, Korea). The size distribution was characterized using a Zetasizer Nano ZS 90 (Malvern,

Worcestershine, UK) at a fixed angle of 90° and temperature of 32°C. Size distribution was also measured by the Zetasizer after 100-fold dilution with water. The turbidity of 100-fold diluted sample was measured by the Turbidimeter (2100N, HACH, Loveland, Colorado). The encapsulation efficiency and quercetin assay were performed by using the standard procedure [22]. The prepared lipid vehicles were separated from the free quercetin using Sephadex G-50 (GE Healthcare) resin and their entrapment efficiency was measured. The entrapment of quercetin into lipid vehicles can be determined by measuring the quercetin elution as a function of time. Free quercetin and the encapsulated quercetin can be separated by Sephadex column. Since the free drug would be trapped in the column, the encapsulated quercetin could be determined by collecting aliquots from the column elution. The quercetin-loaded vehicle of 0.1 mL was loaded into the 2 mL resin. The outflow of the 5 mL PBS was individually collected and measured by spectrophotometry at 369 nm. The entrapment efficiency (EE) of quercetin in the lipid vehicles was calculated as follows:

$$EE = \frac{We}{Wi} \times 100\ \%$$

where Wi was the initial amount of drug added in the lipid vehicles and We was the drug entrapped in the lipid vehicles determined by using Sephadex column. SLNs and NE were diluted 1:25 with Milli-Q water and dried on carbon film (CF200-Cu, Electron Microscopy Science, Washington, PA, USA) for 12 hours. After staining with a 1% solution of phosphotungstic acid (Merck, Darmstadt, Germany) for 30 seconds, samples were then analyzed by Transmission Electron Microscopy (TEM) (JEOL JEM 2000 EXII, Tokyo, Japan). The size distribution of nanoparticles in TEM images was analyzed by Image J software.

2.3. Antioxidant activity assay

Scavenging free radical potentials were tested using methanol solution of DPPH (diphenyl-1-picrylhydrazyl) by Burda and Oleszek [23]. The ability of quercetin-laden nanocarriers to scavenge the diphenyl-1-picrylhydrazyl (DPPH) radical was measured. DPPH (10 mM) was dissolved in 100% methanol. A reference (methanol) or a solution of quercetin-laden nanocarriers (50 µL) was added to 100µL of the DPPH solution, and the spectrophotometric readings (n=3) were taken at 517 nm after 30 min incubation. The antiradical activity (percentage of DPPH decrease) was calculated by using the following equation:

Scavenging effect (%)= [1-(Abs sample / Abs reference)] ×100%

Abs sample: The absorbance of quercetin-laden nanocarriers at 517nm

Abs reference: The absorbance of DPPH in methanol at 517nm

The reducing power of the quercetin was determined according to the method [24]. The quercetin (0.1-40 µg ml^{-1}) was mixed with an equal volume of 0.2 M phosphate buffer, pH 6.6, and 1% potassium ferricyanide. The mixture was incubated at 50 °C for 20 min. Then an equal volume of 10% trichloroacetic acid was

added to the mixture, which was then centrifuged at 6000 rpm for 10 min. The upper layer of solution, distilled water and 0.1% $FeCl_3$ were mixed at a volumetric ratio of 1:1:2. Then the absorbance was measured at 700 nm after 10 min. Increased absorbance of the reaction mixture indicated increased reducing power.

Reducing power (%)= [(Abs sample / Abs vitamin c)] ×100%

The concentration-dependent rate of change in the reducing activity was proportional to the difference between equilibrium antioxidative activity and antioxidative activity at a given antioxidant concentration as follows [24]:

$$Xs = S/S_{Max} \quad (2)$$

$$dXs/dC = K(1-Xs) \quad (3)$$

$$\int_0^{Xs} \frac{dXs}{1-Xs} = -K\int_0^{C} dC \quad (4)$$

$$\ln(1-Xs) = -KC \quad (5)$$

Xs：The fractional reducing activity of the sample

S：The reducing ability of the sample (%)

S_{Max}：The maximal reducing ability of the sample (%)

K：The reaction constant (ml μg^{-1})

C：The antioxidant concentration ($\mu g\ ml^{-1}$)

The half effective concentration (EC_{50}) can be calculated from the antioxidant concentration required for providing 50% of the reducing activity (ie. Xs=0.5) by using the equation (5). A small EC_{50} value represents a high reducing activity. Additionally, a large constant (K) represents a fast reducing reaction.

2.4. Biocompatibility evaluation

SIRC and RGC-5 were respectively maintained in Eagle's Minimum Essential Medium (MEM) and Dulbecco's modified Eagle's medium (DMEM) with 10% fetal bovine serum supplement at a condition of 37℃, 5% CO_2 and 95% relative humidity. After 72 hours, culture medium is removed from the 96-well plate and replaced by 0.1 ml/well quercetin solution for 24 hours. When the medium was removed, 0.5 $mgml^{-1}$ of MTT (dimethylthiazol-2,5-diphenyl tetrazolium bromide) was added to the wells. After incubation at 37℃ for 4 hours, unreacted dye was removed by aspiration. The insoluble formazan crystals were dissolved in 0.2 ml dimethyl sulfoxide. Then the absorbance was measured in a multiple plate reader at 570 nm. The IC_{50} was calculated as the quercetin concentration that inhibits the growth of 50% of the cells relative to non-treated control cells. The protection of quercetin against H_2O_2 was evaluated by using the previous procedure[25, 26]. After the three day culture, the spent media of SIRC and RGC cells was replaced with fresh media. The cells were treated with the flavonoids for 30 minutes before the addition of the oxidant

(H_2O_2).The concentrations of H_2O_2 used in the SIRC and RGC cells were 17.00 and 34.15 μgml^{-1}, respectively.The cell viability was determined by the MTT value at 570 nm after the 24 hour culture.

$$\text{Cell viability (\%)} = \frac{\text{Abs sample}}{\text{Abs control}} \times 100\%$$

2.5. Quercetin accumulation and partition coefficient in ocular tissues

To investigate possible drug penetration or retention in the ocular tissues, the following experiments were performed to measure partition coefficient and accumulation rate of quercetin in the sclera or cornea. The tendency of quercetin into ocular tissue was estimated by measuring its partition coefficient between porcine sclera and the formulation at 32℃, the body surface temperature. Quercetin in the vehicles was fixed at 2000 μg g^{-1}. The quercetin-loaded vehicle solution (2 mL) was mixed with the sclera or cornea (18–22 mg per piece) in a 10 ml vial. The vehicle and the ocular tissues were incubated at the shaker with 200rpm agitation for 4 h. Three pieces of sclera or cornea were randomly withdrawn from the vial, rinsed with phosphate buffer saline, wiped with paper and weighed. The ocular tissue was then homogenized and the quercetin accumulated in tissue was extracted by using 2 mL of the extraction buffer (10% tetrahydrofuran and 90% methanol). Each experiment was replicated at least four times. The homogenized solution was centrifuged at 8000 rpm, filtered by a polypropylene filter (0.45 μm pore size) and analyzed by HPLC to determine the content of quercetin in the tissue. The quercetin concentration in the tissue [C_q] after the incubation period was calculated as follows:

$$C_q = \frac{Wq}{Wt}$$

where Wq was the quercetin in the tissue and Wt was the weight of the tissue. The average thickness of porcine cornea and sclera were 1243.33±60.46 and 968.00±76.00 μm, respectively (n=10). Finally, the partition coefficient was calculated using the equation [27]:

$$\text{partition coefficient} = \frac{Cq}{Ci}$$

where [Ci] was the initial concentration of quercetin (2000 μg g^{-1}) and Cq was the quercetin amount in the tissue by using the HPLC. In vitro permeation and release studies of quercetin were performed in static Franz diffusion cells. The cell consisted of donor and receptor chambers between which a PVDF membrane or a ocular tissue was positioned. A PVDF membrane (Millipore, Germany) with an average pore size of 100nm was used as a barrier to prevent the entrance of nanocarriers to the receptor liquid. Total volume of 1 ml dispersion (containing 2000μg quercetin) was applied to the donor compartment. The composition of simulated tear fluid includes sodium bicarbonate (0.20%), calcium chloride (0.01%), sodium chloride (0.67%) and water (99.12%). The receptor fluid (5.5 mL) consisted of simulated tear: ethanol (4:1) (v/v).

The addition of 20% ethanol in the receptor medium was chosen because of the insufficient solubility of lutein in aqueous buffer. Each receptor chamber contained a stirring magnetic bar to maintain the solution homogeneity. The temperature of receptor chamber was controlled at 32 ◦C by a water circulator. The whole buffer in the receptor chamber was taken and fresh buffer was replenished at fixed intervals. Quercetin in the receptor chamber was analyzed by HPLC. HPLC system (Jasco, Tokyo, Japan) consists of a pump, a UV detector, and a Microsorb-C18 column (Varian, CA, USA). The gradient of mobile phase for quercetin analysis is described as follows. Firstly methanol and 15% acetic acid were mixed with the ratio of 97:3. At 4 min, methanol and 15% acetic acid were mixed with the ratio of 93.5:6.5. At 6 min, methanol and 15% acetic acid were mixed with the ratio of 97:3. The quercetin is well separated at the retention time of 2.83 minutes. The flow rate and detection wavelength is 1.0 ml min^{-1} and 370 nm, respectively [28].

2.6. Confocal and histological examination of porcine eyes

The depth of penetration of quercetin into the corneal tissue is measured by using the confocal microscopy. Porcine sclera or cornea after the diffusion treatment was fixed in PBS solution containing 10% formalin. Tissues were dehydrated sequentially using ethanol and embedded in paraffin. Next, they were sectioned longitudinally by a microtome (Leica RM 2235, Bannockburn, IL, U.S.A.) at 5 μm thickness, and finally stained with hematoxylin and eosin (HE) for histological images. These section samples were then observed under a light microscope (Olympus BX51, Tokyo, Japan) under 40× magnification. When Confocal Laser Scanning Microscopy (CLSM) was used, the sclera or cornea was removed from the diffusion cell and directly observed without wiping the quercetin on tissue surface with the ethanol solution. The sample was immersed in a 1:1 solution of PBS–glycerol, placed between a glass slide and a coverslip and examined by CLSM without additional processing. Fluorescent images were obtained by Leica TCS SP2 CLSM (Leica, Nidau, Switzerland). The fluorescence of quercetin was excited at a wavelength of 488 nm by means of an argon laser. The emission of quercetin was observed within the wavelengths between 500 and 600 nm [29].. To visualize the distribution of quercetin, confocal images were first obtained in the *xy*-plane. The top surface of sample (z=0 μm) was defined as the fluorescence plane with a morphology characteristic of the tissue surface. The tissue was scanned from the top surface (0 μm) to a depth of 75 μm at a 15-μm interval. All images were obtained with the same optical aperture, lens and scan speed.

2.7. Statistical analysis

Data were analyzed using ANOVA Tukey's test in the SPSS package (version 17.0; Chicago, IL, USA). P values of ≤ 0.05 were considered significant and were indicated in the figures. Data were expressed as means ± SD of at least three independent experiments. Multiple comparison procedure was performed using

ANOVA Tukey's test in the SPSS package (version 17.0; Chicago, IL, USA).

3. Results and Discussion

3.1. Characterization and antioxidant activity of quercetin-laden vehicles

The size, polydispersity index, viscosity, entrapment efficacy and turbidity were measured as shown in Table 2. Particle sizes of the developed SLNs and NE were analyzed by using the dynamic light scattering (DLS). The size of the SLNs was significantly larger ($p < 0.05$) than that of the NE. No effect of the lipid source on the quercetin entrapment efficacy was observed ($p > 0.05$) and the efficacy was maintained around 60%. The viscosity and appearance of lipid carriers are important parameters for their application to eyes. The lipid in the formulation attributed to the significant difference ($p < 0.05$) in viscosity and turbidity. TEM was performed to observe the morphology of QT-SLNs and QT-NE (Fig. 1.). QT-SLNs had a large size distribution as compared to QT-NE. NE had diameters of 162.65±31.42 nm which were significantly different from SLNs (324.16±57.38 nm). In contrast, the diameters of QT-SLN and QT-NE by using DLS were 143.0±2.3 and138.3±1.1 nm, respectively (Table 2). The diameter measured by TEM is under the dry condition. Whereas the diameter measured by DLS is in the aqueous solution. The fact that DLS and TEM results are not comparable since the measuring state of nanoparticle was different. The aggregation of solid lipid during the TEM vacuum dry process contributed to the large size. Additionally, TEM also indicated that QT-SLNs had a circle shape but QT-NE had an irregular shape. The results of polydispersity index (PDI) indicated that the size distribution in QT-SLNs and QT-NE was large since the PDI was 25% (Table 2). Zeta potential is an important factor for the stability of nanocarriers. When the zeta potential of a colloidal suspension > ±30mV, the electric repulsion between two colloids can avoid the aggregation and maintain the stability. However, the stability of a colloidal system depends on the balance of the surfactant at the oil–water interface, the nature of the oil phase, the cosolvents in the aqueous and oil phases, the viscosity, and the electro-kinetic properties of the lipid colloids. Blends of hydrophilic and hydrophobic surfactants can increase an emulsion's stability and reduce the size of the oil droplets by reducing interfacial tension between the oil and water phases. Additionally, several nonionic surfactants offer additional steric stabilization effects by avoiding aggregation of the nanoparticles in the colloidal system. Our storage test indicated that the nanocarriers were stable during the 30days. Herein, two surfactants (Tween 40 and Span 40) on the oil-water interfaces and the nano-scale size contributed to the stability of the developed nanocarriers.

The radical scavenging action is one of the mechanisms for antioxidation [30]. DPPH possesses a proton

free radical and shows an adsorption at 517nm. This substrate is used to evaluate the free radical scavenging activity of natural compounds [31]. The purple color of DPPH fades rapidly when it encounters radical scavengers [32]. The dose-dependent response of DPPH assay for quercetin laden vehicles and vitamin C was observed (Fig. 2). Free quercetin had a higher scavenging activity as compared to free vitamin C (control). The scavenging activity of QT-SLNs increased with increasing quercetin concentration to 32μg ml^{-1} and then leveled off with further increase in concentration. The reason that QT-NE and QT-SLNs had minor scavenging effects as compared to that of free quercetin was due to the long distance of quercetin from the lipid core. However, no significant difference ($p>0.05$) existed between the free quercetin and quercetin laden vehicles. The half effective concentration (EC_{50}) can be calculated as the antioxidant concentration required for providing 50% of the antioxidant activity. In Table 3, the radical scavenging ability slightly reduced after encapsulation as indicated in EC_{50} values. The reducing power of antioxidant can be proportional to the ferrocyanide formation [30]. Fig. 3 shows the reducing power of vitamin C, quercetin and quercetin laden vehicles at a 90 μg ml^{-1} level. The formulations were ranked in terms of the reducing activity as QT <QT-NE < QT-SLN. The ferrocyanide formation was maximal when quercetin was encapsulated in SLN. A smaller EC_{50} value represents a higher antioxidant activity. In Table 4, EC_{50} of QT-SLNs (4.25μg ml^{-1}) was better than that of free quercetin (26.17μg ml^{-1}) and QT-NE (18.56μg ml^{-1}). The SLNs had the maximal reducing power, followed by quercetin laden NE and the free quercetin (Table 4). Previously, Lai et al. assumed that the concentration-dependent rate of change in the antioxidative activity was proportional to the difference between equilibrium and real antioxidant activity [24]. Herein, we also adopted the same approach to analyze the antioxidant data. The reaction constant (K) was an indicator for the antioxidant activity. A higher K value represents a higher rate for the scavenging reaction. In the next section, the biocompatibility of QT-NE and QT-SLNs was carried out by using two ocular cell lines. Sequentially, the porcine sclera and cornea were chosen as the target tissues for evaluating the ocular delivery by using QT-NE and QT-SLN.

3.2. Biocompatibility of quercetin-laden vehicles on SIRC and RGC-5 cells

Since very limited information is available for the biocompatible effect of quercetin-laden nanoparticles on ocular cell lines, we adopted SIRC and RGC-5 cells to investigate this impact. The free quercetin and quercetin laden vehicles containing 2000 μg ml^{-1} quercetin were used for the biocompatible experiments. The encapsulation by SLNs and NE could alleviate the cell toxicity of quercetin in both cell lines (Fig. 4). Free quercetin at the 125 μg ml^{-1} level would induce the death of 90% SIRC cells whereas the same payload

in SLNs and NE was non-toxic. Similar protection by nanocarriers was also observed in RGC-5 cells. The best biocompatibility was observed for the QT-SLNs as indicated in Fig. 4 (A) and (B). QT-SLNs had the largest values of half maximal inhibitory concentration (IC_{50}) on the cornea cells (268.9μg ml^{-1}) and retinal ganglion cells (211.3μg ml^{-1}), respectively. Free quercetin owned more toxicity as compared with the QT-SLNs and QT-NE. The IC_{50} of free quercetin on SIRC and RGC-5 cells were 90.5 and 80.1μg ml^{-1} respectively. SLNs had the minimal toxicity when used to encapsulate quercetin as indicated in the IC_{50} results (Fig. 5). In a previous study, stearic acid nanoparticles were cytotoxic at the 1% concentration for mouse J774 macrophages [33]. The solid fat such as a mixture of diglycerides and monoglycerides has been reported to be biocompatible with several cell lines [4]. Our results confirmed that the lipid vehicles containing the lipid and surfactant could modulate the tolerance of quercetin in the two ocular cell lines.

3.3. Protection of quercetin-laden vehicles against H_2O_2 stress on SIRC and RGC-5 cells

RGC-5 cells have been used as an *in vitro* model for the study of neuroprotection by using carotenoids [34]. The protection of coumaric acid on oxidative damage in SIRC cells has been investigated [35]. In order to evaluate the protective efficacy of quercetin-laden vehicles against the H_2O_2 stress, ocular cells such as SIRC and RGC-5 cells were exposed to H_2O_2 in the presence of quercetin-laden vehicles. After 24 hours, cell viability was determined using the MTT assay. At first, the 17 μg ml^{-1} H_2O_2 concentration was chosen in order to inhibit the 80% cell growth. We found that the tolerance of RGC-5 against H_2O_2 was higher than that of SIRC cells (Fig. 6(A) and (B)). A higher concentration of H_2O_2 (34.2 μg ml^{-1}) was used to induce growth inhibition in RGC-5 cells. Our results reveal that two vehicles used to encapsulate the quercetin had great impact on the protective effect of quercetin. The free quercetin (8μg ml^{-1}) could marginally protect the 40% of SIRC cells. No protection was observed against the oxidative stress in RGC-5 cells when free quercetin was used. The large aggregation and limited solubility of free quercetin in the aqueous phase contributed to this fact. In contrast, both QT-SLNs and QT-NE could protect the 95% viable cells of SIRC and RGC-5 in the oxidative stress model at 63μg ml^{-1}. QT-SLNs had better protection as compared to QT-NE. However, the protection of QT-SLNs and QT-NE at the concentration of 125μg ml^{-1} saturated as indicated in the Fig. 6. The eye is constantly exposed to the action of oxidative stress since light-induced photo-oxidative reactions occurs. Tear fluid contains a sufficient amount of scavengers of oxygen free radicals which is capable of intercepting hydroxyl radicals. When the reactive oxygen species overcomes these antioxidant defenses, cell damage can occur [35]. Different mechanisms of quercetin protection have been reported. These include increasing intracellular GSH, lowering levels of reactive oxygen, and

preventing the influx of Ca^{2+} [30]. Quercetin acts directly as an antioxidant, neutralizing toxic ROS by donating hydrogen ions and induces the phase 2 genes Nrf2 and HO-1 that can protect human ocular cells from oxidative stress [25]. Though free quercetin may have the efficacy of cellular internalization, it was observed that QT-SLNs and QT-NE could provide better protection [36] or the sustained release of lipid nanoparticles. Additionally, the use of solid lipids instead of liquid oils can achieve a slow release because drug mobility in a solid lipid should be considerably lower compared with the oil [37].

3.4. Accumulation of quercetin in the ocular tissues by using quercetin-laden vehicles

The accumulation rate, penetration depth and partition coefficient of quercetin in the ocular tissue are important factors for the delivery efficacy. In order to evaluate the ocular quercetin accumulation by using lipid nanocarriers, the porcine cornea and sclera are chosen as *in vitro* models. We investigated the vehicle effect of NE and SLNs on quercetin accumulation in the sclera and cornea during the 4 hour incubation. As shown in Fig. 7, the formulations were ranked in terms of scleral and corneal quercetin accumulation as QT < QT-NE < QT-SLNs. The promotion of the SLNs for quercetin accumulation in the ocular tissue was confirmed. Additionally, quercetin was easier to accumulate in porcine sclera than in cornea in the in vitro model. Sclera could accumulate 5-fold more quercetin as compared to the cornea. The fact that sclera had more quercetin accumulation than cornea may be due to the loose and homogenous structure of sclera. In comparison, the compact cornea contains five layers including epithelium, Bowman's membrane, stroma, Descemet's membrane and the endothelium[38]. The corneal and scleral permeations of quercetin using QT-SLNs and QT-NE were shown in Supplementary Information Fig. S1. The corneal permeation rates of quercetin using QT-SLNs and QT-NE were 158.5 and 130.7 $\mu g\ cm^{-2}\ day^{-1}$, respectively. Whereas the scleral permeation rates by using QT-SLNs and QT-NE were only 9.0 $\mu g\ cm^{-2}\ day^{-1}$.

The partition coefficient of quercetin is important for delivery efficacy since this coefficient provides the accumulation tendency in the targeting tissue. The partition coefficient was measured by using the Franz diffusion cells and by assuming the passive diffusion model between the vehicles and the ocular tissue. The accumulation and partition coefficient of quercetin in the sclera were five-fold higher than in cornea (Table 5). The trend for the quercetin partition in the ocular tissues was similar to that of quercetin accumulation. The partition coefficient of QT-SLNs was significantly higher ($p < 0.05$) than that of QT-NE in both tissues. The quercetin in the cornea saturated after 2 hour diffusion while the quercetin could steadily accumulate in the sclera during the 4 hour period when SLNs were used (Fig. 7). The scleral accumulation of QT-SLNs reached 500 $\mu g\ g^{-1}\ hr^{-1}$. The QT-NE slightly accumulated in the scleral tissues at the level of 200 $\mu g\ g^{-1}\ hr^{-1}$,

and then leveled off with further increase in time. The free quercetin hardly penetrated or accumulated in the sclera and cornea as indicated in Fig. 7 and Fig. 8. QT-SLNs also showed to penetrate more deeply in the sclera (73μm) than QT-NE did (60μm) as indicated in Fig. 8. The confocal microscopic results also indicated that QT-SLNs could diffuse deeply than QT-NE in both sclera and cornea. As shown in Fig. 9, the diffusion depth of quercetin in cornea and sclera increased in the order of QT < QT-NE < QT-SLNs. The localization of quercetin in the sclera or cornea was confirmed by using the CLSM technique. Our CLSM results showed the penetration profiles of quercetin within the ocular tissues were vehicle dependent. The confocal intensity indicated that the quercetin accumulation by SLNs in the sclera or cornea was much higher than that of NE. Since the quercetin partition into the eye is the first step for the accumulation, the improved accumulation of QT-SLNs may be due to the increase in partitioning when SLNs were used as carriers. The quercetin accumulation was enhanced when SLNs were used in the CLSM results. Several factors such as diffusivity coefficient, path length, blood and lymphatic flow and partition coefficient influence the ocular drug accumulation [38]. Herein, we investigated two lipid vehicles for quercetin delivery. Although lipid vehicles have been already applied to deliver ophthalmic drugs, the studies comparing SLNs with NE for quercetin ocular delivery were very limited. SLNs were found to enhance the quercetin encapsulation efficacy and tissue partition (Table 2 and Table 4). Additionally, SLNs had higher viscosity (43 mPa.s) than that of NE (6 mPa.s) as indicated in Table 2. This trend was similar to our earlier investigation for transdermal psoralen delivery [39]. Gallarate et al. enhanced the contact time of cornea with the developed emulsion by optimizing its viscosity [40]. Effect on quercetin accumulation and diffusion by lipid vehicles (Fig. 7, Fig. 8) indicate that the amount of scleral or corneal quercetin accumulation using SLNs was significantly higher than that of quercetin alone. Several mechanisms contributed to the increased scleral delivery by lipid carriers including the enhancement of quercetin solubility, the lipophilic property of lipid and the surface occlusion effect by SLNs [4]. The fact that SLNs had more quercetin accumulation than NE has been attributed to the occlusive effect ensuring close contact and better adhesion on the ocular surface [41]. The solid lipid, glyceryl palmitostearate, has been successfully applied to the ocular drug delivery including Cyclosporine [42] and flurbiprofen [43]. The occlusion factor can enhance the delivery which depends strongly on the crystallinity of the solid lipid matrix, whereas the liquid oil in the nanoemulsion does not have the crystalline property [43]. Finally, the in vitro release results of quercetin in the simulated tear fluid by using the developed nanocarriers are added in Supplementary Information Fig. S2. The data indicated that the quercetin release rate in the simulated tears was 2~4μg hr^{-1}.

Conclusion

Quercetin encapsulated by SLNs and NE was applied to *ex vivo* scleral and corneal delivery by using the porcine eyes. The difference in the composition of two nanocarriers is the lipid. Estasan in QT-NE is a liquid triacrylglyceride containing caprylic and capric fatty acids. Compritol in QT-SLNs is a solid lipid composed of glyceryl dibehenate that is helpful for drug sustained-release. The two lipids contributed to the different characteristics of QT-SLNs and QT-NE in the ocular delivery applications. We found that the radical scavenging and reducing abilities of quercetin were preserved after encapsulation by the lipid nanocarriers. Among the NE and SLNs, the latter showed better performance. The QT-SLNs had the highest flux of 158 $\mu g cm^{-2} day^{-1}$ through cornea using the diffusion device. In addition, QT-SLNs showed significant compatibility with cornea cells (SIRC) and retinal ganglion cells (RGC), and the values of IC_{50} were 268.85 and 211.3 $\mu g ml^{-1}$, respectively. QT-SLNs could efficiently protect cornea and retinal ganglion cells from H_2O_2-induced oxidative damages as compared to free quercetin. The penetration depth in the porcine cornea by using QT-SLNs was 75μm, which showed good results as compared to QT–NE (60μm). Similarly, the corneal permeation fluxes ($\mu g\ cm^{-2}\ day^{-1}$) of quercetin using QT-SLNs and QT-NE were 158.5 and 130.7, respectively. However, the scleral permeation fluxes for both nanocarriers were around the level of 9.0 $\mu g\ cm^{-2}\ day^{-1}$. Our results demonstrated that QT-SLNs were potent for the transocular delivery. However, the *in vivo* experiment using the developed lipid carriers require further investigation.

Acknowledgments

Authors are thankful to the authorities of Chang Gung Memorial Hospital (CMRPD1D0091, 1E0131) for providing necessary facilities and also appreciate the financial support funded by Ministry of Science and Technology, ROC (MOST 103-2221-E-182 -010, 104-2221-E-182-059).

Conflict of Interests

The authors declare that there is no conflict of interests regarding the publication of this paper.

References

1. Y. C. Kim, B. Chiang, X. Wu and M. R. Prausnitz, *Journal of Controlled Release*, 2014, **190**, 172-181.
2. J. G. Souza, K. Dias, T. A. Pereira, D. S. Bernardi and R. F. V. Lopez, *Journal of Pharmacy and Pharmacology*, 2014, **66**, 507-530.
3. L. Gan, J. Wang, M. Jiang, H. Bartlett, D. Ouyang, F. Eperjesi, J. Liu and Y. Gan, *Drug discovery today*, 2013, **18**, 290-297.
4. A. Seyfoddin, J. Shaw and R. Al-Kassas, *Drug delivery*, 2010, **17**, 467-489.
5. A. R. Madureira, D. A. Campos, P. Fonte, S. Nunes, F. Reis, A. M. Gomes, B. Sarmento and M. M. Pintado, *RSC Advances*, 2015, **5**, 22665-22673.

6. X. Hu, X. Kang, X. Ying, L. Wang and Y. Du, *RSC Advances*, 2015, **5**, 40341-40347.
7. R. Liu, Z. Liu, C. Zhang and B. Zhang, *Journal of pharmaceutical sciences*, 2011, **100**, 3186-3195.
8. J. Araujo, E. Gonzalez, M. A. Egea, M. L. Garcia and E. B. Souto, *Nanomedicine : nanotechnology, biology, and medicine*, 2009, **5**, 394-401.
9. A. Shoham, M. Hadziahmetovic, J. L. Dunaief, M. B. Mydlarski and H. M. Schipper, *Free Radical Biology and Medicine*, 2008, **45**, 1047-1055.
10. M. Russo, C. Spagnuolo, I. Tedesco, S. Bilotto and G. L. Russo, *Biochemical Pharmacology*, 2012, **83**, 6-15.
11. J. P. Carini, F. Klamt and V. L. Bassani, *RSC Advances*, 2014, **4**, 3131-3144.
12. M. Stefek and C. Karasu, *Rejuvenation Research*, 2011, **14**, 525-534.
13. N. M. M. Saviranta, L. Veeroos, L. J. Granlund, V. H. Hassinen, K. Kaarniranta and R. O. Karjalainen, *Food Research International*, 2011, **44**, 109-113.
14. J. Romero, G. E. Marak Jr and N. A. Rao, *Ophthalmic Research*, 1989, **21**, 112-117.
15. F. T. M. C. Vicentini, T. R. M. Simi, J. O. Del Ciampo, N. O. Wolga, D. L. Pitol, M. M. Iyomasa, M. V. L. B. Bentley and M. J. V. Fonseca, *European Journal of Pharmaceutics and Biopharmaceutics*, 2008, **69**, 948-957.
16. A. P. Rogerio, C. L. Dora, E. L. Andrade, J. S. Chaves, L. F. C. Silva, E. Lemos-Senna and J. B. Calixto, *Pharmacological Research*, 2010, **61**, 288-297.
17. H. Li, X. Zhao, Y. Ma, G. Zhai, L. Li and H. Lou, *Journal of Controlled Release*, 2009, **133**, 238-244.
18. Y. Gao, Y. Wang, Y. Ma, A. Yu, F. Cai, W. Shao and G. Zhai, *Colloids and Surfaces B: Biointerfaces*, 2009, **71**, 306-314.
19. S. Dhawan, R. Kapil and B. Singh, *Journal of Pharmacy and Pharmacology*, 2011, **63**, 342-351.
20. U. B. Kompella, A. C. Amrite, R. Pacha Ravi and S. A. Durazo, *Progress in retinal and eye research*, 2013, **36**, 172-198.
21. C. H. Liu, K. Y. Lai, W. C. Wu, Y. J. Chen, W. S. Lee and C. Y. Hsu, *Chemical and Pharmaceutical Bulletin*, 2015, **63**, 59-67.
22. C. H. Liu, H. C. Chiu, W. C. Wu, S. L. Sahoo and C. Y. Hsu, *Journal of Ophthalmology*, 2014, **2014**, 304694.
23. S. Burda and W. Oleszek, *Journal of Agricultural and Food Chemistry*, 2001, **49**, 2774-2779.
24. L. S. Lai, S. T. Chou and W. W. Chao, *Journal of Agricultural and Food Chemistry*, 2001, **49**, 963-968.
25. A. Hanneken, F. F. Lin, J. Johnson and P. Maher, *Investigative Ophthalmology and Visual Science*, 2006, **47**, 3164-3177.
26. P. Maher and A. Hanneken, *Investigative ophthalmology & visual science*, 2005, **46**, 4796-4803.
27. H. Wen, J. Hao and S. K. Li, *Pharmaceutical Research*, 2010, **27**, 2446-2456.
28. S. Bose, Y. Du, P. Takhistov and B. Michniak-Kohn, *Int J Pharm*, 2013, **441**, 56-66.
29. A. P. Nifli, P. A. Theodoropoulos, S. Munier, C. Castagnino, E. Roussakis, H. E. Katerinopoulos, J. Vercauteren and E. Castanas, *Journal of Agricultural and Food Chemistry*, 2007, **55**, 2873-2878.
30. K. Ishige, D. Schubert and Y. Sagara, *Free Radical Biology and Medicine*, 2001, **30**, 433-446.
31. K. Shimada, K. Fujikawa, K. Yahara and T. Nakamura, *Journal of Agricultural and Food Chemistry*, 1992, **40**, 945-948.
32. Y. Athukorala, K. N. Kim and Y. J. Jeon, *Food and Chemical Toxicology*, 2006, **44**, 1065-1074.
33. W. Weyenberg, P. Filev, D. Van den Plas, J. Vandervoort, K. De Smet, P. Sollie and A. Ludwig, *International Journal of Pharmaceutics*, 2007, **337**, 291-298.
34. S. Y. Li and A. C. Y. Lo, *International Journal of Molecular Sciences*, 2010, **11**, 2109-2117.
35. M. Lodovici, L. Raimondi, F. Guglielmi, S. Gemignani and P. Dolara, *Toxicology*, 2003, **184**,

141-147.
36. H. Kettiger, A. Schipanski, P. Wick and J. Huwyler, *International journal of nanomedicine*, 2013, **8**, 3255-3269.
37. W. Mehnert and K. Mäder, *Advanced drug delivery reviews*, 2001, **47**, 165-196.
38. V. P. Ranta, E. Mannermaa, K. Lummepuro, A. Subrizi, A. Laukkanen, M. Antopolsky, L. Murtomaki, M. Hornof and A. Urtti, *Journal of Controlled Release*, 2010, **148**, 42-48.
39. J.-Y. Fang, C.-L. Fang, C.-H. Liu and Y.-H. Su, *European Journal of Pharmaceutics and Biopharmaceutics*, 2008, **70**, 633-640.
40. M. Gallarate, D. Chirio, R. Bussano, E. Peira, L. Battaglia, F. Baratta and M. Trotta, *Int J Pharm*, 2013, **440**, 126-134.
41. S. Wissing and R. Müller, *International journal of pharmaceutics*, 2002, **242**, 377-379.
42. E. Wolska and M. Sznitowska, *Int J Pharm*, 2013, **441**, 449-457.
43. E. Gonzalez-Mira, S. Nikoli, A. C. Calpena, M. A. Egea, E. B. Souto and M. L. Garcia, *Journal of pharmaceutical sciences*, 2012, **101**, 707-725.

Table 1. The composition of quercetin-laden vehicles

	Percentage (wt %)					
	Quercetin	Estasan	Compritol® 888 ATO	Tween® 40	Span® 40	Water
QT-NE	0.2	2	-	2.5	2.5	92.8
QT-SLN	0.2	-	2	2.5	2.5	92.8

Table 2. Characteristics of quercetin-laden vehicles

	QT-SLN	QT-NE
Z-average (nm)	143.0±2.3*	138.3±1.1*
Polydispersity index	0.27±0.04	0.25±0.01
Viscosity (mPa · s)	43.34±0.04*	6.14±0.00*
Zeta potential (mV)	-16.57±0.57*	-23.97±1.75*
Entrapment efficiency (%)	66.56±6.62	74.26±4.53
Surface tension (mN/m)	14.71±0.45	14.69±0.33
Turbidity (NTU)	136.33±2.08*	256.33±8.39*

*Significant statistical difference compared between QT-SLNs and QT-NE. ($p<0.05$, n = 3)

Table 3. Parameters of antiradical activity (DPPH) for quercetin-laden vehicles

	EC_{50} * (μg ml^{-1})	K (ml/μg)	R^2
QT	11.83	0.1095	0.9068
QT-NE	14.83	0.0710	0.9688
QT-SLN	17.13	0.0695	0.9777
Vitamin C	13.60	0.0874	0.9178

*$EC_{50,}$ half maximal effective concentration

Table 4. Parameters of reducing power for quercetin-laden vehicles*

	EC_{50} * (μg ml^{-1})	K (ml/μg)	R^2
QT	26.17	0.0293	0.8714
QT-NE	18.56	0.0325	0.9898
QT-SLN	4.25	0.0732	0.9151

*$EC_{50,}$ half maximal effective concentration

Table 5. The partition coefficient and accumulation of quercetin in porcine ocular tissues *

		QT	QT-NE	QT-SLN
Cornea	Accumulation (μg g^{-1})	66.8±5.1	144.6±4.0*	357.9±137.0*
	Partition coefficient	0.033±0.003	0.072±0.002*	0.179±0.068*
Sclera	Accumulation (μg g^{-1})	221.0±18.4	497.7±72.2*	2100.0±43.9*
	Partition coefficient	0.111±0.009	0.474±0.219*	1.050±0.022*

*Significant statistical difference compared to free QT. ($p<0.05$, n = 3)

Partition coefficient = accumulation of quercetin in tissue (μg g^{-1}) / initial concentration of quercetin (μg g^{-1}) after 4 hours.

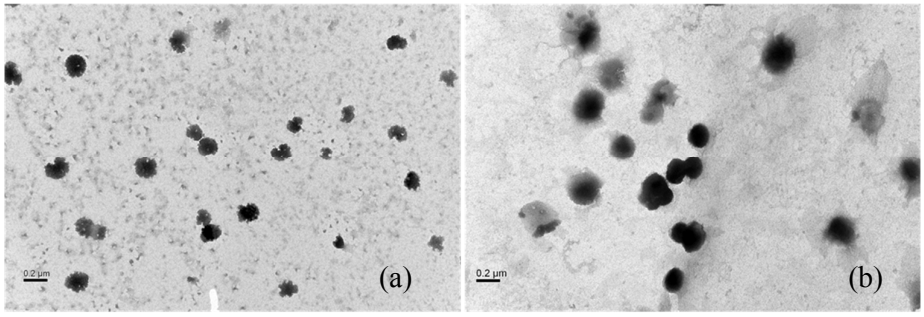

Fig 1. TEM images of quercetin-laden vehicles (a) QT-NE (mean diameter=162.65±31.42 nm, n=18), (b) QT-SLN(mean diameter=324.16±57.38 nm, n=14).The scale bar represents 200 nm length.

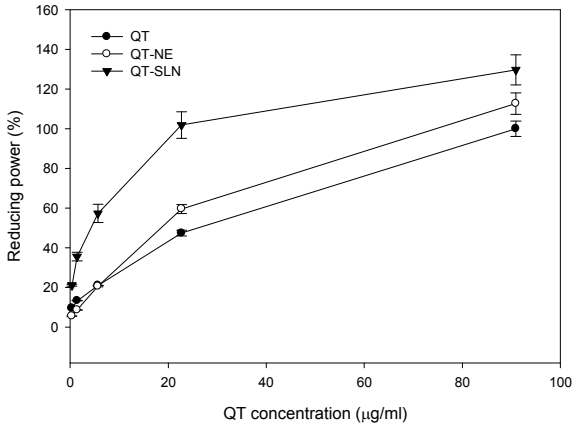

Fig. 2. The reducing power of quercetin-laden vehicles. (n = 3)

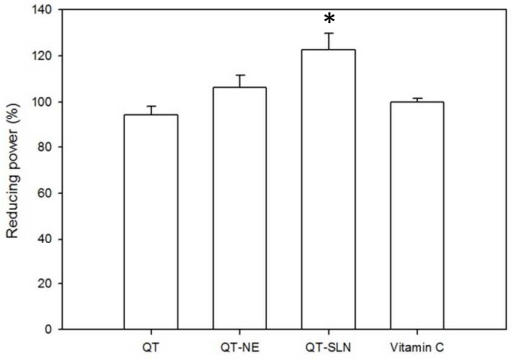

Fig. 3. The reducing power of quercetin-laden vehicles at the concentration of 90 μg ml^{-1}. Vitamin C (90 μg ml^{-1}) was used as the control. *Significant statistical difference compared to Vitamin C ($p<0.05$, n = 3).

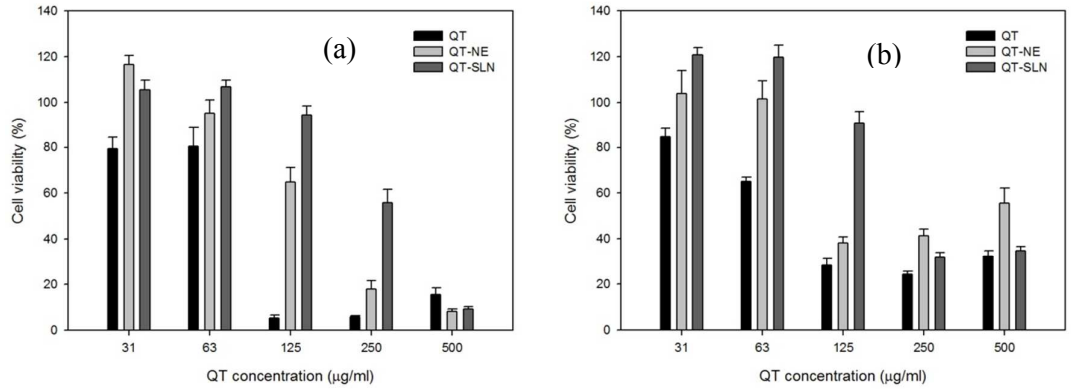

Fig. 4. The biocompatibility of quercetin-laden vehicles in ocular cells (a)SIRC (b)RGC-5. (n = 5)

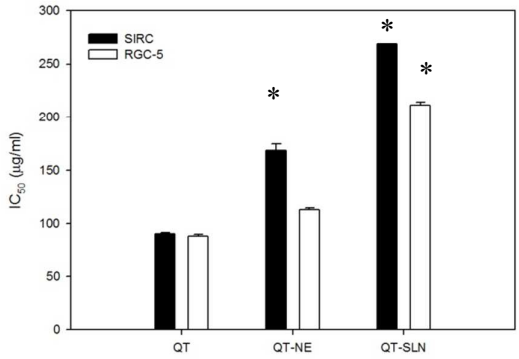

Fig. 5. The half maximal inhibitory concentration of quercetin-laden vehicles in SIRC and RGC-5 cells. *Significant statistical difference compared to quercetin ($p<0.05$, n = 5).

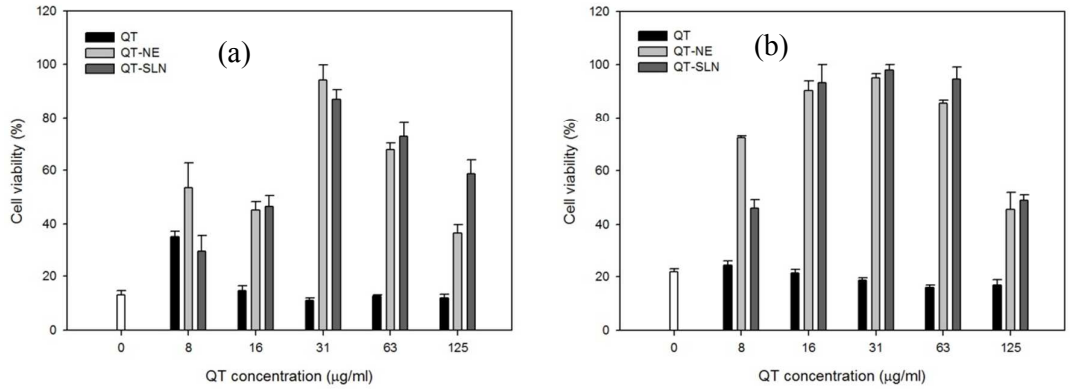

Fig. 6. The protection of quercetin-laden vehicles against H_2O_2 in the ocular cells. (a)SIRC was treated with 17.00 μg $ml^{-1}H_2O_2$ (b)RGC-5 was treated with 34.20 μg ml^{-1} H_2O_2. n=5

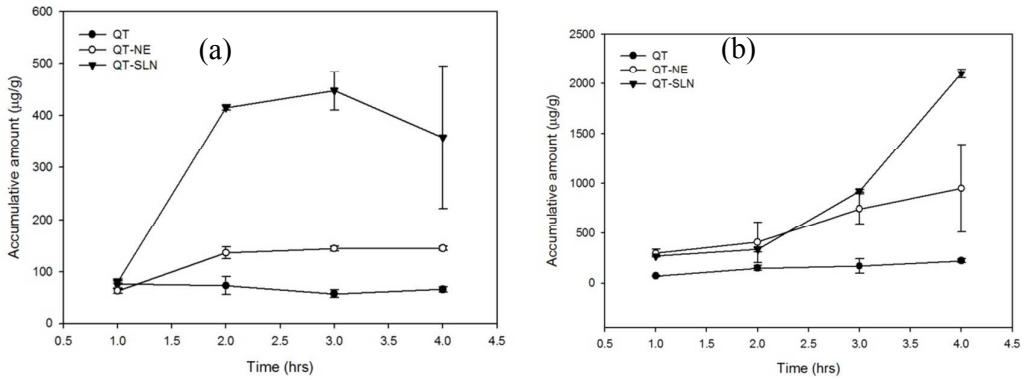

Fig. 7. The 4-hour accumulation of quercetin in porcine ocular tissues by using quercetin-laden vehicles in cornea (a) and sclera (b)

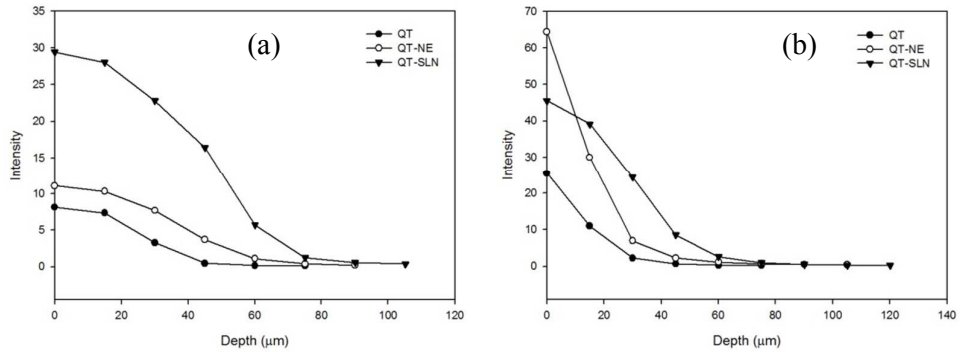

Fig. 8. Penetration depth of quercetin in porcine ocular tissues by using quercetin-laden vehicles after 12-hour treatment, cornea (a) and sclera (b)

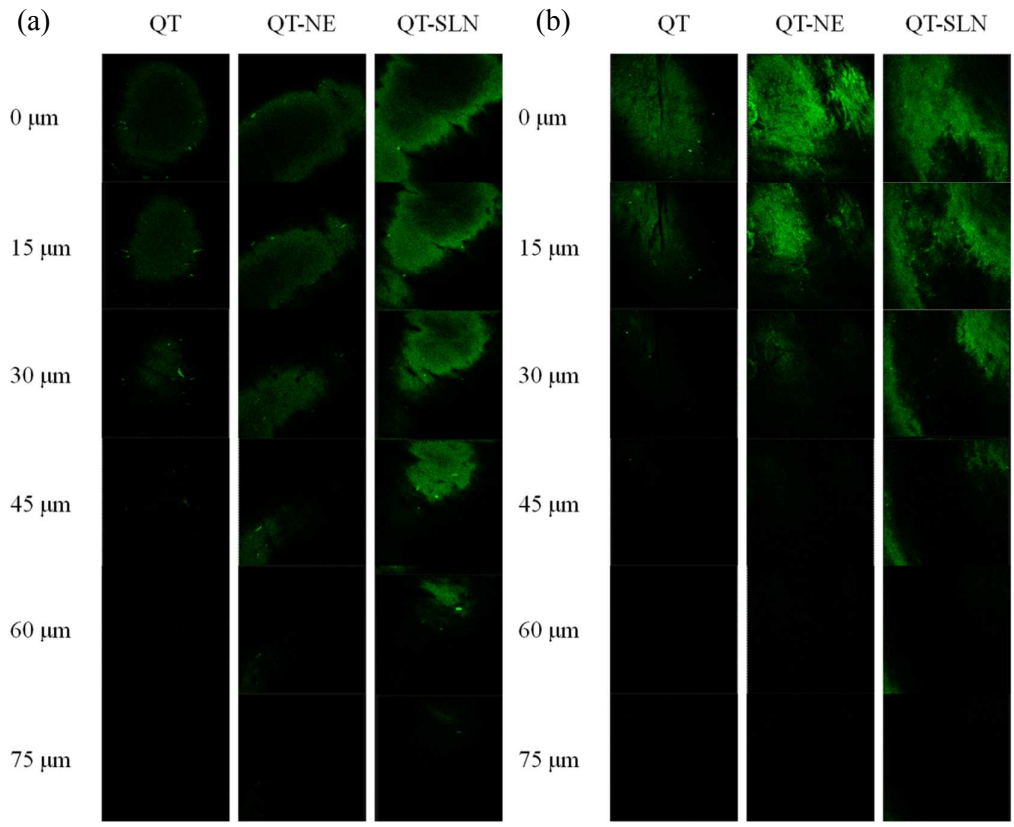

Fig. 9. Quercetin distribution in porcine ocular tissues after 12-h treatment using confocal laser scanning microscopy, cornea (a) and sclera (b). Fluorescence of quercetin emitted at 515 nm was recorded when excited at a wavelength of 488 nm by means of an argon laser. The sample was scanned from the tissue surface (0 um) to a depth of 75μm at a 15 μm interval.

Quercetin delivery by lipid nanoparticles